A Programmable Transmission Electron Detector for Nanomaterials Characterization in a Scanning Electron Microscope

Jason Holm* (jason.holm@nist.gov), Benjamin Caplins*, Robert R. Keller*
*National Institute of Standards and Technology, Boulder, CO, USA.

ABSTRACT

A new programmable detector for scanning transmission electron microscopy (p-STEM) is described. A digital micromirror array lies at the heart of the detector and serves as a programmable virtual objective aperture. Two sensors, a photomultiplier tube and a CMOS digital camera, are used to enable real-space transmission imaging and on-axis diffraction, respectively. Detector operation is demonstrated with several samples in a conventional scanning electron microscope (SEM).

Keywords: scanning, transmission, electron microscopy, diffraction, programmable

INTRODUCTION

Scanning electron microscopes (SEMs) are ubiquitous in materials analysis labs because the focused electron probe can provide useful information about diverse samples on different length scales. Although usually considered a tool best suited for topographical imaging with secondary electrons, SEMs are well-suited for imaging nanomaterials with transmitted electrons. Compared to electron energies typically used for transmission imaging (i.e., $\geq$ 100 keV), the energies typical of SEM electrons (i.e., $\leq$ 30 keV) enable stronger interaction between the electron probe and the sample, which means more information can be obtained in some instances. Despite recent advances to better utilize the transmitted electron signal in SEMs [1,2], part of the reason this signal has not been more diligently pursued is that for thicker samples, plural- and multiple-scattering events make transmission signals challenging to interpret quantitatively. For nanomaterials, single-scattering is highly probable for many samples at typical SEM energies, and theories developed for conventional transmission electron microscopy could be utilized if a detector capable of selecting specific signals were available. To that end, this contribution describes a programmable scanning transmission electron microscope (p-STEM) detector that enables imaging and diffraction in an SEM [3,4]. Although nanomaterials are used to demonstrate detector operation in this work, any sample sufficiently thin to allow electrons through can be used.

STEM DETECTOR

An overview of the detector is provided here, and more detailed descriptions can be found in the literature [3,4]. Fig. 1a shows the p-STEM detector attached to an SEM, and Fig. 1b shows a closer view of some of the components for comparison with Fig. 1c, where the signal path is illustrated. The detector works as follows: A convergent electron beam (e^-) is rastered across a sample. If the sample is sufficiently thin, electrons will pass through the sample. Some of the transmitted electrons might scatter due to interactions with the sample. Transmitted electrons, both scattered and unscattered, that strike the phosphor with sufficient energy will cause photon emission. Part of that photon signal is then reflected outside the SEM vacuum chamber by a mirror and through a short lens assembly (optics) to a 1024×768 array of micromirrors. The micromirror array, or digital micromirror device (DMD), serves as a virtual objective aperture that enables the user to direct the transmitted electron signal (i.e., the photons) through another short lens assembly (optics) to either detector 1 (D1) or detector 2 (D2). Here, D1 is a CMOS digital camera used for recording images of diffraction patterns, and D2 is a photomultiplier tube (PMT) used for real-space STEM imaging. Signals from D1 and D2 can be recorded and displayed multiple ways. For example, the PMT can be used as an auxiliary input that is directly synchronized with the SEM imaging system much like a conventional Everhart-Thornley electron detector. Alternatively, both signals can be digitally acquired external to the SEM and displayed/modified/analyzed by use of non-proprietary software.

The DMD is central to detector programmability and novelty. Each micromirror can be tilted to any one of three positions including off (i.e., no tilt) and ±12 degrees (i.e., up towards D1 or down towards D2). Essentially, the array serves as an electronically configurable, virtual objective aperture that can take on any user-defined shape on the fly. Virtual aperture geometries can be created numerous ways. In the current configuration, digital images are programmed to the DMD to tilt the mirrors in the desired direction. For example, Fig. 2a shows a 1024×768 black and white image of a small annulus. Each white pixel in the image will be used to command the corresponding mirror in the DMD array to tilt towards the PMT, black pixels will tilt mirrors towards the CMOS camera. Figure 2b shows a closer view of the DMD mirror array with the annulus image programmed to it. Individual mirrors can be observed (13.7 μm squares), and those that are bright are tilted towards the PMT, thereby forming a virtual annular aperture for real-space imaging. In this configuration, the only signal reaching the PMT will be whatever is reflected by the virtual annular aperture. More specifically, this aperture was

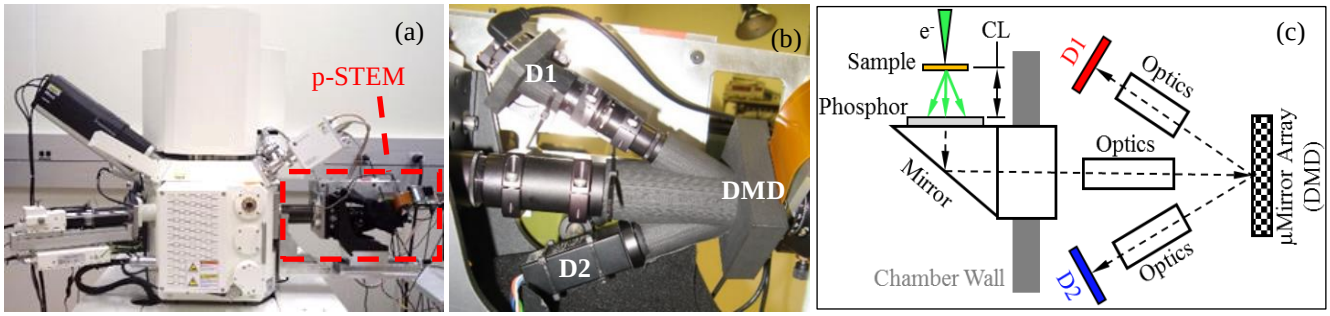

Figure 1: (a) A prototype programmable STEM detector for the SEM. (b) A closer view of some components. Optical paths are covered to block stray light. (c) Signal path schematic. Electron paths are shown in green (color online), photon paths are shown by the dashed lines. This embodiment of the detector employs a digital camera as D1 and a photomultiplier as D2.

programmed for low angle annular dark-field (ADF) imaging with electrons scattered between 5 mrad and 10 mrad. Digital images programmed to the DMD need not be limited to conventional round, annular, or segmented annular geometries, but any pattern can be programmed to the DMD, meaning that most conventional transmission imaging modes can be implemented, and new imaging modes can easily be explored. For example, rather than using a single round aperture for ADF imaging, multiple apertures can be used to simultaneously capture signals from multiple diffraction spots. Moreover, the ability to automate imaging with user-programmable scripts is feasible either with the DMD software or with other commercial or open-source software.

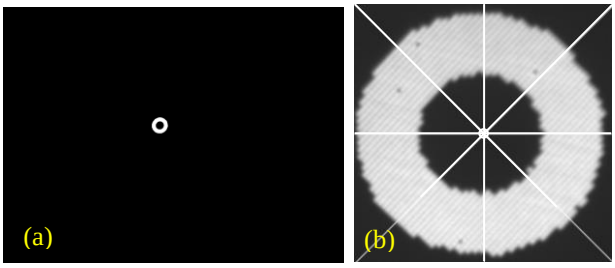

Figure 2: (a) An image of a small annulus to be programmed to the DMD array for low angle ADF imaging. (b) An image of the DMD mirror array recorded in the SEM. White pixels are mirrors tilted towards the PMT, and crosshairs indicate the optic axis.

DETECTOR OPERATION

An important first operation is detector alignment, several of which may be necessary depending on the goal of the imaging session. Coarse mechanical alignment is accomplished with an *xyz*-positioning stage on the detector. The purpose here is to approximately center the DMD array on the optic axis, and to optimize the space between the phosphor and the SEM pole piece (i.e., to maximize the available camera length, CL). Another alignment involves positioning the virtual objective aperture(s). For example, the annular pattern in Fig. 2b is nearly centered on the optic axis, but the annulus is not centered in the digital image programmed to the DMD (Fig. 2a), nor does it need to be. Although the virtual apertures can be positioned mechanically using the *xyz*-positioning stage, it is much easier to position them electronically by tilting different mirrors. A more critical alignment, perhaps, is between the object plane and the detector image plane. (Note that the phosphor is effectively the object plane.) This step is required to ensure that STEM images and diffraction patterns are not rotated, distorted, or otherwise out of alignment with each other, and that objects in images recorded with other SEM detectors align with objects recorded in STEM images. These image/object plane misalignments are determined electronically [4], and if desired, corrections can be automatically applied to images and diffraction patterns via straightforward image processing.

Basic STEM imaging and the detector novelty are demonstrated in Fig. 3 which shows images of carbon nanotube synthesis byproducts deposited on a lacey carbon substrate. A large agglomerate of amorphous carbon is visible in the secondary electron (SE) image (Fig. 3a), and faint spots (presumably catalyst particles) can be observed within individual globules. To better identify and define the spots, conventional bright-field (Fig. 3b) and ADF (Fig. 3c) images can be recorded with the p-STEM detector. (Actual images of the different virtual apertures programmed to the DMD are shown.) Contrast observed in Figs. 3b and 3c suggests that the particles are of different composition than the amorphous carbon. To better discern the materials, diffraction patterns can be recorded from individual particles by tilting all of the DMD mirrors towards the CMOS camera, positioning the electron beam at desired locations in the image, and recording images of the scattering patterns (i.e., the diffraction patterns in Fig. 3b) with the camera. For these diffraction patterns, Fig. 3b was used to select the spots at which to position the beam, but an image of the sample from any detector on the SEM could also be used. Diffraction patterns collected from three spots suggest the particles are crystalline and the surrounding globular material is amorphous.

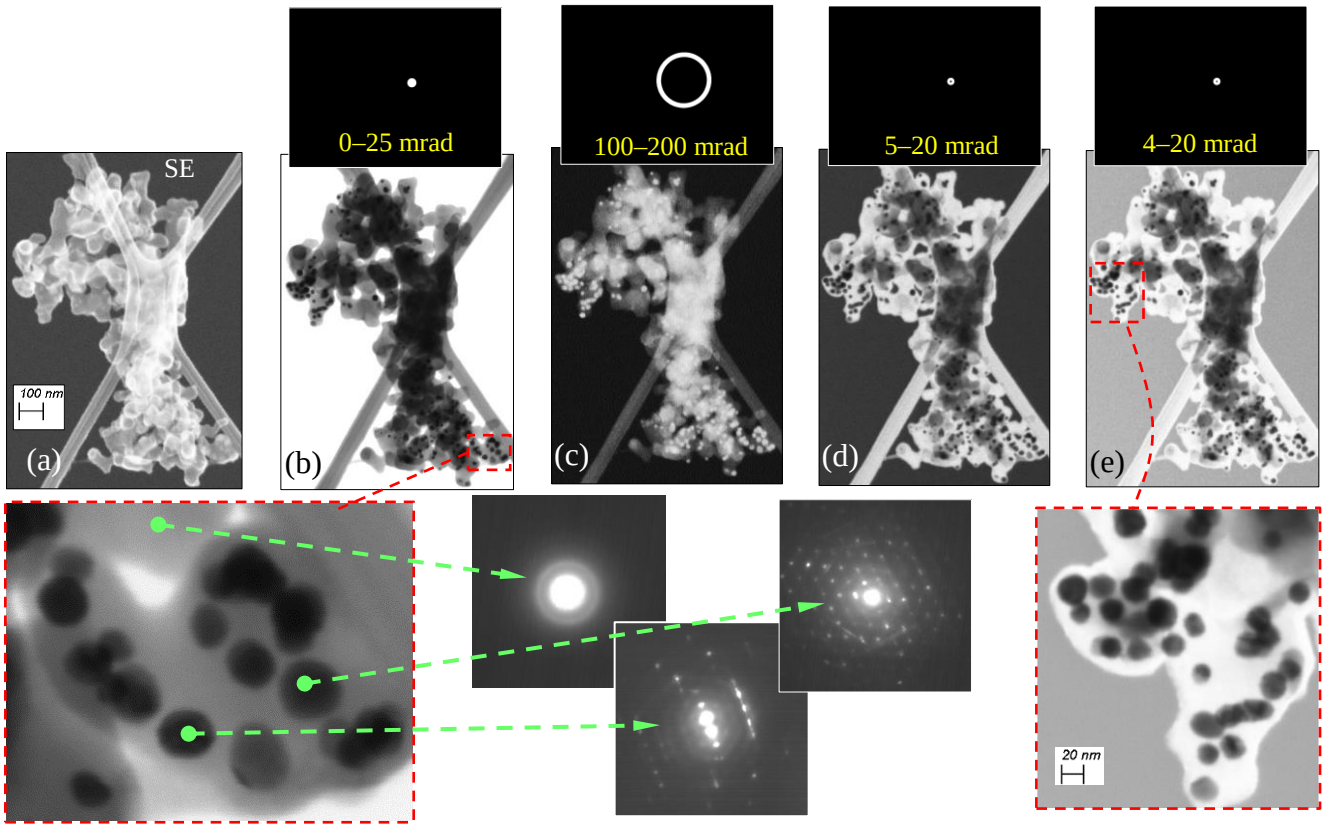

Figure 3: Various images of carbon nanotube synthesis byproducts. Virtual apertures are shown above their respective STEM image. (a) A secondary electron image. (b) Conventional bright-field STEM images and diffraction patterns from the indicated spots. (c) An ADF image showing Z-contrast. (d) and (e) Marginal bright-field images with slightly different inner acceptance angles.

Figs. 3d and 3e show additional detector utility. Two nearly identical apertures were programmed to the DMD to demonstrate marginal bright-field imaging, a mode enabling simultaneous observation of low-Z and high-Z elements. Here, the catalyst particles can be easily discerned from the amorphous carbon, and a closer view (Fig. 3e) reveals contrast variation suggestive of structural inhomogeneity within many particles. Perhaps the most apparent difference between the two images, however, is the background. At 5 mrad (Fig. 3d), the background is dark because the signal from the direct beam is blocked by the virtual aperture. At 4 mrad (Fig. 3e), the background is brighter because the virtual aperture allows part of the direct beam to contribute to the image signal. By varying the inner radius of the virtual aperture, the electron beam convergence angle can be quantified. So, in addition to enabling nonconventional imaging modes, the detector can also be used to glean information about the SEM.

Diffraction patterns can also be obtained from large areas within a given image. This is important for beam-sensitive materials like the zeolites shown in Figure 4. Here, ~4.6 nm thick zeolite sheets [5] were imaged in ADF mode with the indicated aperture image (30 mrad – 250 mrad) programmed to the DMD. The rectangular areas of adventitious carbon indicate the areas from which the diffraction patterns were obtained. Total integration time for each diffraction pattern was ~2 s with very short pixel dwell time. The importance of detector alignment is also demonstrated. For example, zeolites in the ADF image exhibit a distinct orientation that the diffraction pattern should replicate. To that end, the inset diffraction pattern

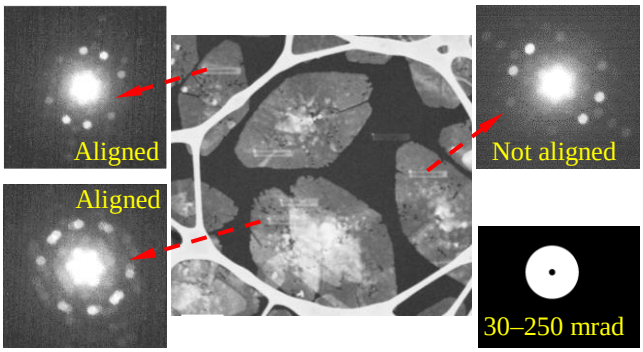

Figure 4: A STEM image of 2D zeolites using a mrad 30 mrad – 250 mrad virtual annular aperture and various diffraction patterns.

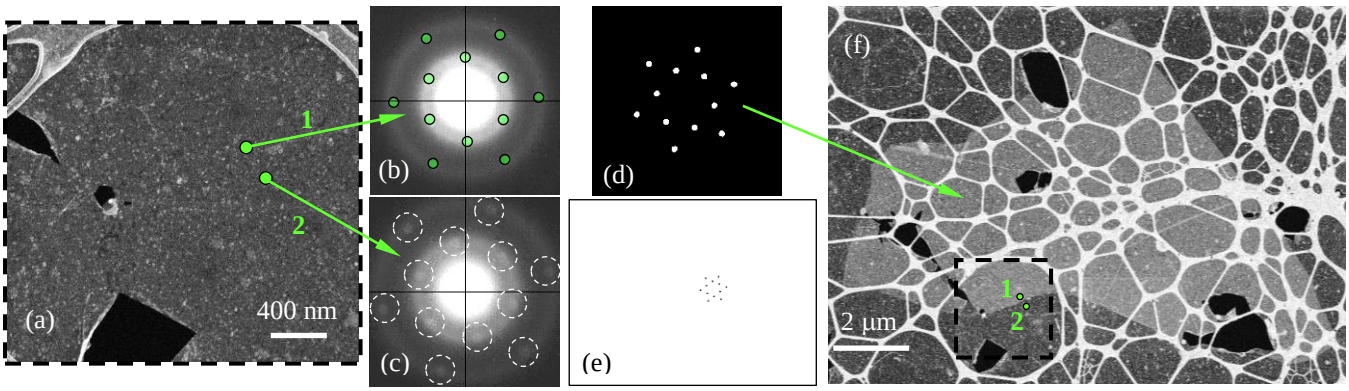

Figure 5: Visualizing grain orientation in monolayer graphene. (a) An SE image recorded with an Everhart-Thornley detector. (b) A diffraction pattern obtained at point 1. Green circles are drawn over the twelve faint diffraction spots. (c) A diffraction pattern obtained at point 2. Twelve faint diffraction spots can be observed within the dashed circles. (d) A close-up view of the digital image used to program a virtual aperture based on the spots in (b). (e) The entire digital image used to program a virtual aperture based on diffraction pattern in (c). Colors are reversed to enable spot visualization. (f) A dark-field image obtained using the virtual aperture in (d). A single large grain is revealed as the bright continuous area.

on the top-right is shown without applying the detector alignment correction. The pattern does not align well with the zeolite sheet. Detector misalignment was accounted for in the other two diffraction patterns, and both are well-aligned with the sheets as they appear in the real-space image. Also, notice that the diffraction pattern in the lower-left was recorded from an area of two overlapping and slightly rotated sheets. The slightly rotated spot sets can be used to estimate the relative rotation between the two sheets.

A last example demonstrates one way to simultaneously implement multiple virtual apertures for samples that do not scatter electrons strongly. Fig. 5a shows an SE image of dirty monolayer graphene with a few torn areas. Two points were chosen in this image and diffraction patterns were obtained at those locations with the p-STEM detector (Figs. 5b and 5c). Twelve faint, but distinct spots can be observed in each diffraction pattern, and the 12-spot patterns are rotated with respect to each other by ~10.5 degrees. Twelve small circles, each corresponding to a distinct 4 mrad aperture, were then drawn over the 12 spots in both images (i.e., Fig. 5c, green circles, color online), and two virtual aperture image files (Figs. 5d and 5e) with similar but slightly rotated spot patterns were generated based on those patterns. (Note: only a small portion of the virtual aperture image file is shown in Fig. 5d. For illustrative purposes, the full virtual aperture image file programmed to the DMD is shown for diffraction pattern two in Fig. 5e.) Then, with the image files programmed to the DMD, real-space dark-field images were recorded using the PMT. For example, the image in Fig. 5f was obtained with the virtual aperture in Fig. 5d and shows a large continuous bright region that represents a single grain of graphene. The real-space image (not shown) obtained with the virtual aperture in Fig. 5e indicates the surrounding graphene is all rotated ~10.5 degrees with respect to the large central grain. As might be anticipated based on these results, mapping grain orientation automatically over very large areas is feasible with this detector [6].

SUMMARY

A new programmable detector has been described that enables transmission electron imaging and diffraction with any or all of the transmitted electron signal. The examples presented here demonstrate that detector alignment is important, and that the detector can be operated in conventional and nonconventional imaging modes. Moreover, the potential to explore and develop new imaging modes and contrast mechanisms with this detector is high.

REFERENCES

[1] Keller, R. R. and Geiss, R., J. Microsc. 245 (2012) 245-251.
[2] Sun et al., Microsc. Microanal. 24 (2018) 99-106.
[3] Jacobson, B. T. et al., Proc. of SPIE 9376 (2015) 93760K. https://doi.org/10.1117/12.2083520
[4] Caplins, B.W., Holm, J.D., Keller, R.R., Ultramicroscopy 196 (2019) 40-48.
[5] Jeon, M.Y. et al., Nature 543, 690-694.
[6] Caplins, B. et al., Proc. of SPIE 10932 (2019) 109320E. https://doi.org/10.1117/12.2508694